Separation and Purification Technology 377 (2025) 134380

Contents lists available at ScienceDirect

Separation and Purification Technology

journal homepage: www.elsevier.com/locate/seppur

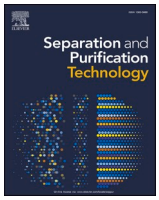

Deactivation of activated carbon during low-temperature NO adsorption-regeneration cycles

Zhongwei Li, Xingyu Yang, Qiang Song [1,*]

Key Laboratory of Thermal Science and Power Engineering of Ministry of Education, Tsinghua University, Beijing 100084, China

ARTICLE INFO

Editor: Philiswa Nomngongo

Keywords:
NO
Activated carbon
Adsorption and regeneration
Deactivation
Flue gas

ABSTRACT

Activated carbon (AC) exhibits excellent NO_x adsorption performance at low temperatures, based on which a cold oxidation adsorption process (COAP) technology has been proposed and demonstrated the capacity of near-zero pollutant emission from flue gas. To explore the deactivation of AC during adsorption-regeneration cycles for COAP, cyclic adsorption (−20℃) and temperature-programmed regeneration (up to 500℃) experiments were conducted for AC. NO_x adsorption capacity was found to drop by 11.4 % after the first four cycles, stabilizing thereafter. The decrease was primarily attributed to an 84.7 % decline in chemisorption, while physisorption remains nearly constant after a minor initial decrease during the first cycle. Temperature-programmed desorption (TPD) analysis revealed the depletion of NO adsorption sites during cycles. XPS characterization identified the change in functional groups (carbonyl, hydroxyl, ether, carbon edge defects) on the AC surface, with edge defects declining sharply and hydroxyl groups remaining stable. NO_x chemisorption proceeds via NO oxidation and NO_2 conversion. TPD and XPS results confirm that the NO oxidation activity is unchanged during cycling. Thus, the decrease of NO_x chemisorption was attributed predominantly to the decay of adsorption sites during NO_2 conversion. Quantum chemical calculations confirmed that among various NO_2 adsorption sites, configurations formed on unsaturated carbon atoms underwent irreversible structural changes during regeneration, forming stable C=O bonds. The irreversible conversion of unsaturated carbon sites was identified as the primary cause of chemisorption capacity loss. Surface modifications are proposed to improve the stabilization of AC's adsorption performance during cycles.

1. Introduction

NO_x is a flue gas pollutant that contributes to environmental problems such as acid rain and photochemical smog [1–3]. Selective catalytic reduction (SCR) has been established as the dominant technology for NO_x emission reduction in coal-fired power plants [4]. However, its application in other industrial sectors (e.g., iron and steel metallurgy) faces substantial challenges, primarily due to temperature incompatibility and high operational costs [5–9]. In metallurgical industries, activated carbon (AC) adsorption technology has been applied for the removal of SO_2, while demonstrating promising potential for simultaneous NO_x abatement.

Activated carbon (AC) possesses a well-developed porous structure that provides exceptional adsorption capacity. However, its adsorption capacity for NO is notably limited. Through catalytic oxidation, NO and O_2 can be converted to NO_2, which has a greater adsorption capacity on AC surfaces. Under conventional medium–low flue gas temperatures, AC's catalytic performance remains constrained. Surface modification techniques, including loading of transition metal oxides (MnO_x, CuO) or KOH impregnation, have been demonstrated to enhance NO_x adsorption capacity by 26–400 % [10–13]. Nevertheless, these modification approaches substantially increase both material costs and process complexity. Furthermore, modified AC often exhibits significant performance declines during adsorption-regeneration cycles, potentially leading to deactivation and elevated operational costs [14]. An alternative strategy involves lowering the adsorption temperature. Experimental studies have shown that reducing the temperature from 20℃ to −20℃ increases NO adsorption capacity by 2.73 times (4.42 mmol/g) [15]. The decrease in temperature leads to an increase in the adsorption of NO and O_2 on the surface of the activated carbon, which promotes the oxidation of NO to produce NO_2. This will lead to a significant increase in the adsorption of NO_2 on the surface of the activated carbon.

* Corresponding author at: Department of Energy and Power Engineering, Tsinghua University, Haidian District, Beijing 100084, China.
E-mail address: qsong@tsinghua.edu.cn (Q. Song).
[1] ResearcherID: U-4938-2019.

https://doi.org/10.1016/j.seppur.2025.134380
Received 11 May 2025; Received in revised form 7 July 2025; Accepted 16 July 2025
Available online 16 July 2025

During NO_x adsorption on AC, O_2 and NO are initially catalytically oxygenated at the active sites adjacent to the hydroxyl functional groups to produce NO_2, as reported in previous studies [16,17]. Some of the NO_2 generated will be chemisorbed, and some will be physically adsorbed. The decrease of adsorption temperature on the one hand leads to a significant enhancement of the NO catalytic oxidation. On the other hand, the NO_2 chemisorption and physisorption capacity of activated carbon is also significantly increased [17], thus realizing the efficient removal of NO_x by AC.

During the adsorption process, both physical and chemical adsorption sites on activated carbon gradually become saturated, eventually resulting in deactivation. To minimize the substantial cost increase caused by frequent adsorbent replacement, thermal regeneration methods are commonly employed for adsorbent recovery. In this process, AC is heated under inert gas purging. Physically adsorbed NO_x rapidly desorbs as the partial pressure in the gas phase decreases. Meanwhile, the chemically adsorbed NO_x undergoes bond cleavage at elevated temperatures, and are subsequently released into the gas stream [16,18–21]. Regeneration is achieved when all adsorbed NO_x species desorb and the active sites are recovered.

However, a gradual decline in adsorption capacity is observed when AC undergoes multiple adsorption-regeneration cycles. Zhang et al. [22] observed a 33.3 % reduction in NO_x adsorption capacity after three cycles of adsorption at 50℃ and regeneration at 300℃. Similarly, Atkinson et al. [23] found a 65.1 % decrease in NO_2 breakthrough time after four cycles of adsorption at 50℃ with regeneration at 400℃. These experiments indicate that activated carbon is gradually deactivated during cycles. Although previous research has observed this deactivation process, the exact mechanisms remain uncertain, with proposed explanations about surface functional group changes lacking experimental verification. Revealing the deactivation mechanism of activated carbon during repeated adsorption-regeneration cycles is crucial for enhancing its performance through modification.

AC exhibits excellent NO_x adsorption performance at low temperatures. Based on this, China Huaneng Group Co., Ltd. proposed a Cold Oxidation Adsorption Process (COAP) technology. The technology is capable of synergistic removal of multiple pollutants, including NO_x. Industrial tests have demonstrated its feasibility for near-zero emission of multiple pollutants. The technology's efficient gradient utilization and recovery of thermal energy significantly improve overall efficiency while reducing consumption, demonstrating strong application potential. However, the evolution of adsorption activity during low-temperature adsorption (−20℃) and medium-temperature regeneration (500℃) cycles remains poorly understood. Elucidating the deactivation mechanisms is critical for developing modified AC materials with enhanced cyclic stability and optimizing regeneration processes for industrial applications. This study systematically investigates the adsorption-regeneration behavior of AC through isothermal adsorption experiments at −20℃ combined with temperature-programmed regeneration. The physicochemical characteristics of cycled AC samples were explored for structural changes, while quantum chemical calculations were employed to reveal the fundamental deactivation mechanisms. The results offer valuable insights into the performance decline during cyclic operations and establish guidelines for developing modified AC with improved low-temperature adsorption stability.

2. Method

2.1. Experimental

2.1.1. Sample

Activated carbon (AC) samples were sourced from Jiangsu JSW Environmental Technology Co., Ltd., China. Before the experiment, the samples were degassed at 200℃ for 2 h to desorb water in the pores. The ultimate analysis and physical properties of the sample are presented in Table 1. A specific description of the measurement methodology can be found in a previous study [17].

Table 1
Ultimate analysis and physical properties of the sample.

Ultimate analysis / wt. %					Specific surface area / $m^2 \cdot g^{-1}$	Total pore volume / $cm^3 \cdot g^{-1}$	Average pore diameter / nm
C	H	O	N	S			
86.3	0.6	13.0	0.0	0.1	823	0.450	2.188

2.1.2. Adsorption and regeneration experiments

The adsorption-regeneration cycle experiments consist of two phases: adsorption and regeneration. Each complete cycle involves one adsorption experiment in the constant temperature system, followed by one regeneration experiment in the fixed bed desorption system.

Adsorption experiments were conducted using a constant-temperature adsorption system (Fig. 1). The U-tube reactor, cooling bath, and heat transfer medium specifications are detailed in reference [17]. The U-tube was submerged in the cooling medium, containing 0.1 g of AC sample secured between quartz wool plugs in the vertical section to prevent movement. The system was maintained at −20℃ using a cryostatic bath. A total gas flow ($NO/O_2/N_2$) of 500 NmL/min was introduced, with individual flow rates accurately regulated by mass flow controllers. The gas mixture first passes through a spiral pre-cooling coil immersed in the cooling medium before entering the temperature-equilibrated U-tube. The reactor outlet gas composition was continuously analyzed using Fourier transform infrared spectroscopy (FTIR; Nicolet 6700, Thermo Fisher Scientific, USA), maintaining measurement accuracy within 3 %. Adsorption experiments concluded after 120 min or when the outlet gas concentrations reached equilibrium.

Due to the 99℃ temperature limitation of the reaction bath being insufficient for complete NO_x desorption from the activated carbon, a two-stage desorption process was implemented, with detailed methodology following the approach described in reference [17]. The first stage of desorption was performed in the low-temperature reaction bath. Following adsorption completion, the gas supply was switched to N_2 for purging through the U-tube. The temperature of the reaction bath was adjusted in the process of purging so that the temperature of the sample was increased from the adsorption temperature T to 30℃ until it stabilized. The first desorption stage was considered complete when the outlet NO_x concentration fell below 10 ppm. During this phase, the released nitrogen oxides primarily resulted from physical desorption of weakly adsorbed NO_x molecules due to the reduced partial pressure in the N_2 atmosphere. The second stage of the desorption was conducted in a fixed-bed desorption experimental system. The AC samples that completed the first stage of desorption were moved to the fixed-bed adsorption experimental system for temperature-programmed desorption experiments. N_2 was used as the purge gas at 200 NmL/min during the second desorption stage. The second stage of desorption was completed by setting the furnace heating program to heat the samples from 30℃ to 500℃ at 10℃/min (no NO_x was removed at this temperature). The second-stage NO_x desorption curve reveals that significant desorption begins near 100 °C, demonstrating that this stage primarily involves chemically adsorbed NO_x. Experimental observations showed minimal NO_x desorption when increasing the temperature from adsorption conditions to 30 °C during purging. Substantial desorption only commenced near 100 °C. Based on these findings, we categorized NO_x released below 30 °C as physically adsorbed and NO_x desorbed between 30–500 °C as chemically adsorbed for analytical purposes.

The fixed-bed desorption system is illustrated in Fig. 2. The quartz sample holder, located in the furnace's isothermal zone, incorporates a quartz sieve plate and high-purity quartz filter membrane (MK360, Munktell, Sweden) for sample support. The holder is sealed with a ground-glass joint at the top of the inner quartz tube. Additional system parameters are detailed in Reference [16]. During operation, gas flows

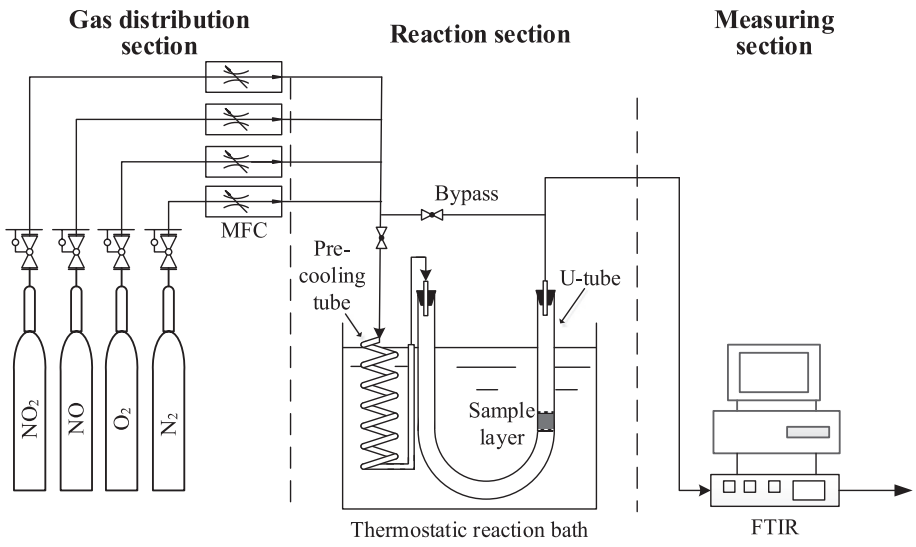

Fig. 1. Schematic diagram of the isothermal adsorption experimental system.

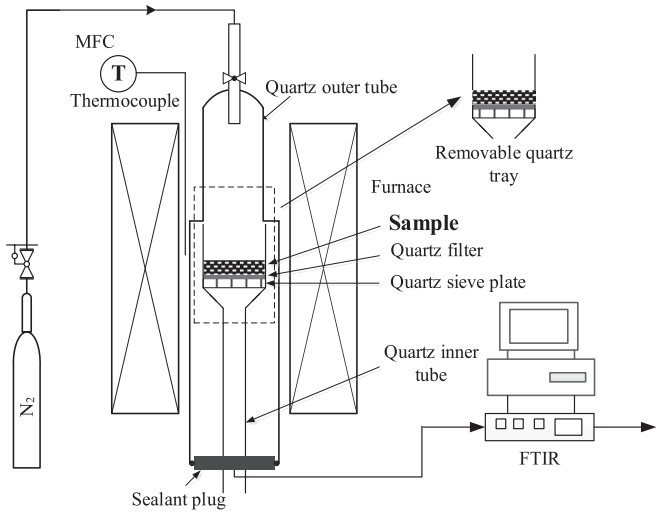

Fig. 2. Schematic diagram of the fixed-bed desorption experimental system.

through the outer quartz tube, permeates the sample bed, and exits via the inner tube's bottom for FTIR analysis.

During the adsorption and regeneration experiments, FTIR only detected two types of nitrogen oxides, nitric oxide and nitrogen dioxide. Based on the variation in the concentration of nitric oxide and nitrogen dioxide in the outlet gas over time, equation (1) was used to calculate the adsorption amount of activated carbon, equation (2) was used to calculate the physical adsorption amount and equation (3) was used to calculate the chemical adsorption amount.

$$N_{NO_x,a} = \int_0^{t_a} \left(\frac{(C_{NO,in} - C_{NO,out} - C_{NO_2,out}) \times 10^{-6} \times Q}{V_m \times m}\right) dt \quad (1)$$

$$N_{NO_x,pa} = \int_0^{t_{pa}} \left(\frac{(C_{NO,out} + C_{NO_2,out}) \times 10^{-6} \times Q}{V_m \times m}\right) dt \quad (2)$$

$$N_{NO_x,ca} = \int_0^{t_{ca}} \left(\frac{(C_{NO,out} + C_{NO_2,out}) \times 10^{-6} \times Q}{V_m \times m}\right) dt \quad (3)$$

Where $N_{NO_x,a}$, $N_{NO_x,pa}$, and $N_{NO_x,ca}$ respectively represent the adsorption amount, physical adsorption amount, and chemical adsorption amount of NO_x on the AC (mmol·g^{-1}). The integration limits t_a, t_{pa}, and t_{ca} respectively represent the time required for the completion of adsorption experiments, desorption stage 1, and desorption stage 2 experiments (s). $C_{NO,in}$, $C_{NO,out}$, and $C_{NO_2,out}$ represent the nitric oxide concentration in the reactor inlet gas, the nitric oxide concentration in the reactor outlet gas, and the nitrogen dioxide concentration in the outlet gas (ppm), respectively. Q represents the gas flow rate (NmL·s^{-1}), V_m represents the molar volume at 0℃ (22.4 L·mol^{-1}), and m represents the loading amount of activated carbon (g).

The initial activated carbon samples (AC_{cyclei}) used for each cycle were characterized for their physical properties using surface analyzers, with specific characterization methods described in section 2.1.1. Surface chemical properties of activated carbon were analyzed with the X-ray photoelectron spectroscopy (XPS; ESCALAB 250Xi, ThermoFisher, U.K.). The O1s binding energy of AC was analyzed with an Al Kα anode. The XPS profiles were calibrated using the C1s (284.8 eV) curve.

2.2. Calculation details

2.2.1. Structural models

The freshly activated carbon was characterized by XPS, and its O1s spectrum is shown in Fig. 3. The spectrum was decomposed into five peaks centered at 530 eV, 532.3 eV, 533.5 eV, 534.3 eV, and 536.3 eV

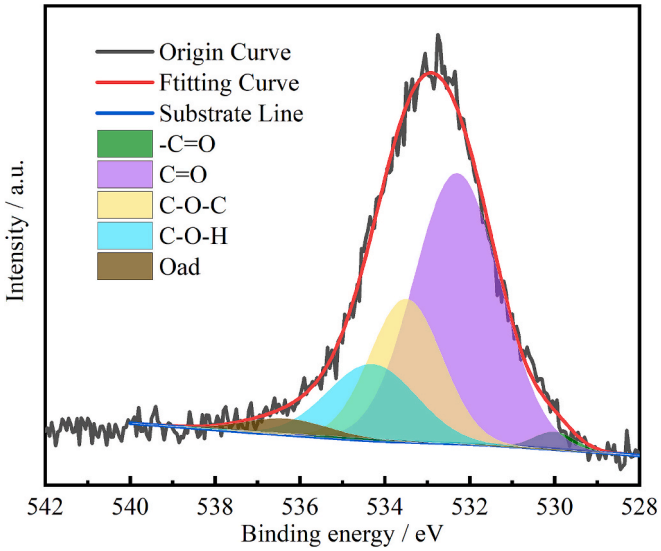

Fig. 3. High-resolution O1s spectra of AC_{cycle1}.

corresponding to −C=O (carboxyl), C=O (carbonyl), C-O-C (ether), C-O–H (hydroxyl), and O_{ad} (water) [24,25], where the content of carboxylic acid and oxygen atoms was extremely low, which indicates that carbonyl, hydroxyl and ether groups are the main oxygen-containing functional groups present on the surface of the activated carbon samples used in this paper.

The amorphous properties of activated carbon were represented through carbon cluster models. A 7-aromatic-ring carbon model was constructed as the baseline configuration (Fig. 4a), selected based on literature evidence [26–28] demonstrating sufficient size to minimize edge effects while balancing computational accuracy and efficiency. To simulate intrinsic defect sites arising from mechanical processing (e.g., ball milling), unsaturated carbon atoms were introduced into the pristine carbonaceous model (Fig. 4b). Three modified models were subsequently developed by incorporating carbonyl, hydroxyl, and ether groups (Fig. 4c-e) [24,27–31]. These carbon models enabled computational analysis of NO and NO_2 decomposition during desorption from their adsorbed configurations at these active sites, helping elucidate the activated carbon deactivation mechanism during cyclic adsorption-regeneration.

2.2.2. Computational methods

All quantum chemical calculations were completed using Gaussian 16 [32]. Geometry optimizations and frequency analyses were conducted at the B3LYP/6-31G(d) level to ensure minimum-energy configurations with no imaginary frequencies. Transition states along reaction pathways were identified via the quadratic synchronous transit (QST) method and validated by the presence of a single imaginary frequency. Intrinsic reaction coordinate (IRC) calculations were carried out to confirm the connectivity between each transition state and adjacent energy minima. Single-point energies for adsorption analysis were computed at the higher-accuracy B3LYP/6-311G(d,p) level.

The adsorption energy of the adsorption configuration was calculated using Equation (4):

$$E_{ad} = E_{complex} - E_{gas} - E_{mod\ el} \quad (4)$$

Where E_{ad} represents the adsorption energy ($kJ{\cdot}mol^{-1}$). $E_{complex}$, E_{gas}, and E_{model} respectively represent the single-point energies ($kJ{\cdot}mol^{-1}$) of the adsorption configuration formed after gas molecule adsorption, the gas molecule, and the carbonaceous model.

All the visualizations of the carbonaceous model in this paper are implemented using Multiwfn software [33].

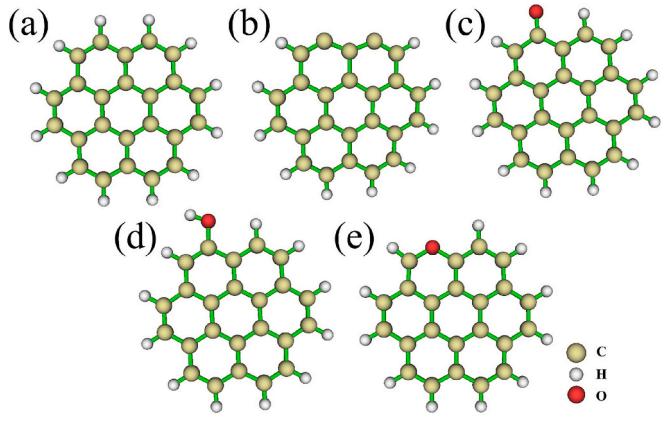

Fig. 4. (a) Pristine carbonaceous model, carbonaceous models containing (b) unsaturated carbon atoms, (c) carbonyl functional group, (d) hydroxyl functional group, and (e) ether functional group.

3. Results and discussion

3.1. Adsorption-regeneration cycle characteristics

The adsorption, physisorption, and chemisorption of NO_x by activated carbon in different cycles are presented in Fig. 5a. The total adsorption amount decreased by 11.4 % (from 1.516 to 1.254 mmol/g) during the first four cycles, with only a marginal 0.4 % decrease (0.005 mmol/g) from the fourth to the tenth cycle, indicating the stabilization of AC activity. The physiosorbed quantity showed negligible changes after the first cycle, with an initial 7.0 % decrease (0.037 mmol/g) followed by stable values in subsequent cycles. In contrast, the chemisorption amount demonstrated a significant decrease (22.5 %, 0.987 to 0.765 mmol/g) during the first four cycles, accounting for 84.7 % of the total adsorption amount loss. This also indicates that the decrease in NO_x adsorption mainly results from the weakening of chemisorbed NO_x. Since chemisorbed NO_x requires specific active sites on the activated carbon surface, we hypothesize that repeated adsorption-regeneration cycles will progressively reduce these sites, leading to a corresponding decrease in NO_x chemisorption capacity.

The adsorption characteristic curves of different cycles of NO_x were observed to further analyze the changes in NO_x adsorption. The adsorption amount (total NO_x, physical adsorption, and chemical adsorption) showed negligible variation between the fourth and tenth cycles. Therefore, only the first five cycles were analyzed for the later cycles in the subsequent analysis as a substitute. The outlet gas analysis during adsorption experiments detected only NO and NO_2 as the nitrogen oxide species present. NO_2 remained undetectable until 67 min of adsorption, after which its concentration exhibited a gradual increase, confirming that NO is oxidized to NO_2, which then adsorbs to the AC surface. The adsorption characteristic curves for NO are shown as solid lines in Fig. 5b, and the adsorption characteristic curves for NO_x ($NO + NO_2$) are shown as dashed lines in Fig. 5b. As adsorption proceeds, the NO_x concentration gradually increases, which corresponds to a decrease in the NO_x adsorption rate. The NO concentration at the reactor outlet showed an increasing tendency of multiple accelerations followed by decelerations in each cycle. With increasing cycle numbers, the outlet NO concentration showed a progressive rise during the 120-minute adsorption period. Specifically, concentrations increased from 124 ppm to 136 ppm during the first four cycles, then stabilized thereafter. This pattern demonstrates progressive AC deactivation during initial cycles, reaching a stable inactive state after four cycles. According to the literature [16], the NO adsorption mechanism includes two stages: NO oxidation and NO_2 conversion. The increasing NO outlet concentration results from two processes: NO oxidation and progressive NO_2 adsorption saturation. As adsorbed NO_2 partially converts back to NO, this creates an initial acceleration followed by deceleration in the NO concentration profile. The consistent NO concentration patterns across cycles confirm that the adsorption mechanism remains unchanged, aligning with previous reports [16].

To elucidate the progressive decline in NO_x chemisorption amount, TPD analysis was conducted. The outlet concentration profiles of NO and NO_2 during desorption are presented in Fig. 6. The desorbed gas contained only NO and NO_2, with Fig. 6a and 6b showing their respective desorption profiles across multiple cycles.

In Fig. 6a, the activated carbon sample AC_{cycle1} exhibits NO desorption peaks at 225℃ (highest), 275℃ (second highest), and 375℃ (lowest). With cycling, peaks at 225℃ and 375℃ gradually decline, while the 275℃ peak vanishes. Taking AC_{cycle5} as an example, the NO desorption profile showed significant changes compared to AC_{cycle1}: the 225 °C peak decreased from 976 to 836 ppm, the 275 °C peak disappeared completely, and the 375 °C peak declined from 165 to 71 ppm. In Fig. 6b, the activated carbon sample AC_{cycle1} exhibits a NO_2 desorption peak near 200℃. As the adsorption-regeneration cycle progresses, the height of the NO_2 desorption peak remains almost unchanged, all around 987 ppm. Based on previous studies [16,17] and the

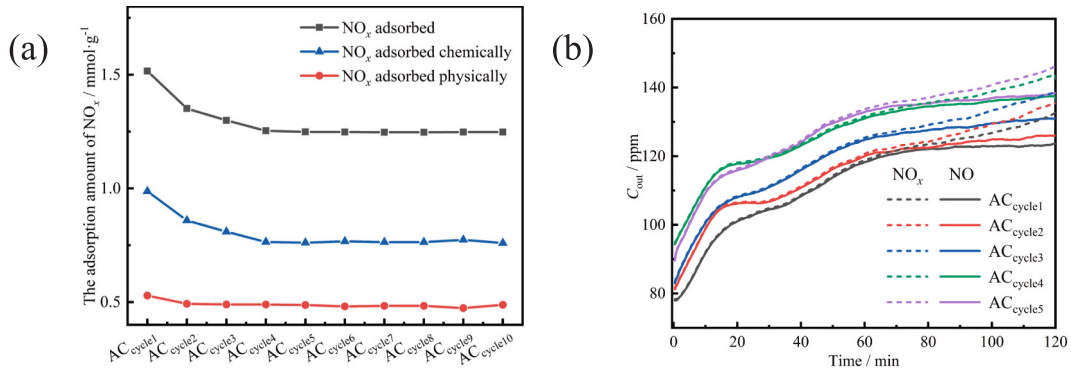

Fig. 5. (a)Total adsorption, physical adsorption, and chemical adsorption amounts of activated carbon, and (b) variation of NO outlet concentration with time in adsorption experiments during adsorption and regeneration cycles.

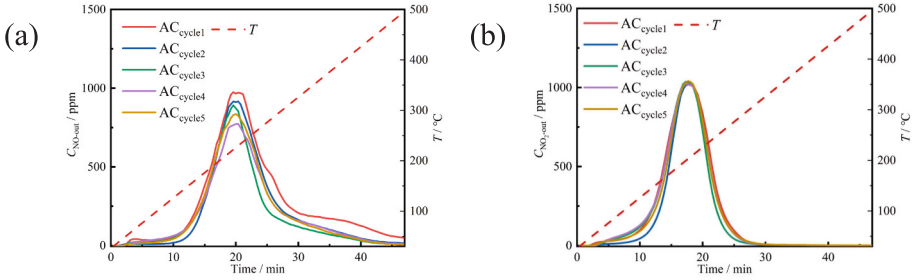

Fig. 6. (a) NO desorption curves and (b) NO_2 desorption curves of activated carbon in temperature-programmed desorption experiments during adsorption-regeneration cycles.

introduction section, NO oxidation and NO_2 adsorption and conversion on activated carbon surfaces have been well described. During temperature-programmed desorption, rising temperatures induce the decomposition of adsorbed NO_x species, yielding both NO and NO_2 through distinct desorption pathways. The stable NO_2 desorption peak intensity across cycles (~987 ppm at 200 °C) corresponds to adsorbed NO_3^- species on saturated carbon sites, as established in previous work [16]. This persistent signal indicates the adsorption-regeneration process does not significantly alter the active sites or configurations involved in NO_3^- formation. Moreover, since the generation of NO_3^- involves NO oxidation, it is speculated that the adsorption-regeneration cycle has little effect on NO oxidation and the active sites (active atoms adjacent to the hydroxyl functional groups) where NO oxidation occurs. The decrease in the NO_x desorption peak reveals another class of NO_x chemisorption sites other than hydroxyl groups – possibly reactive carbon atoms adjacent to oxygen-containing functional groups (carbonyls, ethers) and unsaturated/saturated carbon sites [16]. These sites are gradually deactivated during cyclic operation. The progressive loss of active sites causes a corresponding decline in chemisorption capacity during repeated adsorption-regeneration cycles.

To investigate the variation in NO_x physisorption amount, the physical properties of activated carbon samples were systematically characterized through the first five adsorption-regeneration cycles (Table 2). A marginal increase in total surface area and a slight decline in average pore diameter were observed exclusively after the first adsorption-regeneration cycle, while other physical properties remained largely unaffected. This phenomenon is attributed to the partial conversion of macropores to mesopores during initial regeneration, which marginally reduced average pore size while slightly increasing surface area. Notably, micropore structures remained intact throughout all cycles. Subsequent cycles (2–5) exhibited negligible changes in physical properties, indicating AC structural stabilization after the first regeneration. The physical adsorption of NO_x involves gas diffusion through AC pores to internal surfaces, making the pore structure a critical factor influencing adsorption kinetics through its effect on molecular transport rates. Pore structure characterization revealed that the reduced average pore diameter after the first cycle slowed NO_x diffusion to adsorption sites, accounting for the observed 7.0 % decrease in physisorption capacity. The stabilization of physical properties in subsequent cycles corresponded with consistent physisorption measurements, indicating that pore structure alterations were primarily confined to the initial cycle.

Table 2
The physical properties of activated carbon samples.

	Specific surface area / $m^2 \cdot g^{-1}$	Micropore specific surface area / $m^2 \cdot g^{-1}$	Total pore volume / $cm^3 \cdot g^{-1}$	Micropore volume / $cm^3 \cdot g^{-1}$	Average pore diameter / nm
AC_{cycle1}	822.77	693.13	0.450	0.359	2.188
AC_{cycle2}	858.49	695.22	0.454	0.360	2.169
AC_{cycle3}	855.87	692.32	0.464	0.359	2.168
AC_{cycle4}	854.64	692.00	0.467	0.369	2.166
AC_{cycle5}	856.01	690.53	0.461	0.361	2.174

To better reveal the reasons for the changes in the chemical adsorption of NO_x, XPS characterization was conducted on the activated carbon samples from the first five cycles. XPS analysis of five AC samples revealed consistent surface functional groups, including carbon edge defects, ether (C-O-C), carbonyl (C=O), and hydroxyl (–OH) groups, using identical peak deconvolution methods. Given that ether groups (C-O-C) remain stable below 600 °C, their content was essentially unchanged during the 500 °C regeneration cycles [34,35]. To clearly illustrate the relative changes in functional group composition, Fig. 7 presents the normalized peak area ratios of all identified surface groups relative to the ether group reference. It was found that the carbon edge defects gradually decreased, C-O showed an overall decreasing trend, C-O–H (hydroxyl group) did not change much, and C=O (carbonyl group) gradually increased. Previous studies [16,17,36] identified carbon edge

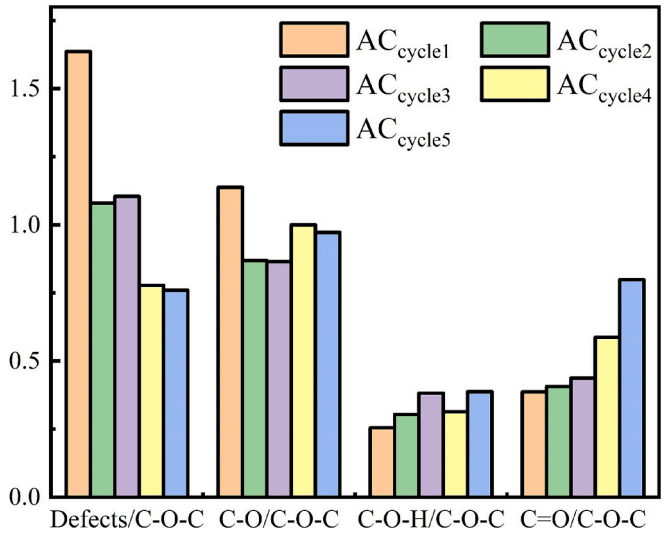

Fig. 7. Distributions of surface functional groups for ACs.

defects, C-O, ether (C-O-C), and carbonyl (C=O) groups as NO_2 chemisorption sites. Our results suggest the declining NO_x chemisorption capacity during cycling primarily results from progressive loss of carbon edge defects, rather than changes in oxygen-containing functional groups. The active atoms near C-O–H are the active sites for NO oxidation, which can carry out a continuous NO oxidation reaction. XPS analysis revealed that oxygen-containing functional groups (C-O, C-O-C, C=O) maintained relatively constant surface concentrations throughout cycling. This stability correlates with the invariant NO_3^- desorption peaks in TPD profiles, indicating that the adsorption-regeneration cycle does not affect the NO oxidation reaction, as well as the sites where the NO oxidation occurs (the active atoms adjacent to the hydroxyl functional group).

3.2. Deactivation mechanism of activated carbon during adsorption-regeneration cycles

Previous studies have demonstrated that activated carbon exhibits negligible direct NO adsorption capacity, relying instead on a two-stage NO oxidation and NO_2 conversion mechanism for NO_x removal [16].

The impact of the adsorption-regeneration cycles on the phase of NO oxidation is first analyzed. As described in the literature [16] and in the introduction section, NO oxidation on the surface of activated carbon occurs on active atoms in the vicinity of hydroxyl functional groups. Based on the analysis in Section 3.1, on the one hand, the TPD experiments revealed that the desorption peaks corresponding to NO_3^- were almost unaffected by the adsorption regeneration cycle, and that the generation of NO_3^- involved the oxidation of NO. This suggests that the adsorption-regeneration cycle has little effect on NO oxidation reactions and hydroxyl functional groups. On the other hand, XPS characterization also indicates that the C-O–H (hydroxyl group) does not change much with adsorption regeneration cycles. From the point of view of the change of adsorption amount with the number of cycles, the physical adsorption of NO_x by activated carbon did not change much in each cycle except the first cycle. Because activated carbon surface physical adsorption of NO_x is mainly NO_2 [17], and NO_2 is all generated by the oxidation of NO. Therefore, this is also able to show that the adsorption regeneration cycle has little effect on the NO oxidation reaction.

Next, the impact of the adsorption-regeneration cycle on the NO_2 conversion stage was analyzed. After NO oxidation, NO_2 will be physiosorbed or chemisorbed on the surface of activated carbon. Through multiple adsorption-regeneration cycles, the activated carbon's total NO_x adsorption capacity showed an initial decline followed by stabilization. While physisorption decreased slightly during the first cycle, then remained constant, chemisorption – accounting for 84.7 % of the total reduction – followed the same trend as the overall adsorption capacity. This dominant contribution indicates that the adsorption capacity decrease primarily stems from changes in chemisorption behavior, allowing us to focus subsequent investigation on chemical adsorption mechanisms while reasonably neglecting minor physical adsorption effects. Previous studies [16] have explored the active site for NO_2 chemisorption, including active atoms near oxygen-containing functional groups (hydroxyl, carbonyl, and ether), unsaturated carbon atoms, and saturated carbon atoms. To elucidate the deactivation mechanisms of specific chemisorption sites, we will perform quantum chemical calculations to further reveal the change of each chemisorption active site during the adsorption-regeneration cycle.

The active atoms adjacent to the hydroxyl group are discussed first. From the previous analysis, it can be seen that the active atoms adjacent to the hydroxyl group do not decrease in the adsorption-regeneration cycle. NO_2 adsorption at these sites was found to produce both N-down and O-down adsorption configurations, which could desorb directly as NO_2 with energies of −61.65 and −70.89 kJ/mol, respectively. Alternatively, computational results revealed that adsorbed NO_2 may decompose and release NO into the gas phase, as illustrated in Fig. 8. The N-down NO_2 adsorption pathway depicted in Fig. 8a involves sequential transformations through multiple intermediates. The process initiates with a 2.3 kJ/mol energy barrier to form IM1, followed by transitions to IM2 and IM3 requiring 104.6 kJ/mol and 10.1 kJ/mol barriers, respectively. During the IM3 stage, progressive elongation of the O-C bond occurs until cleavage at 79.5 kJ/mol, yielding IM4. The final step overcomes a 7.6 kJ/mol barrier to release NO into the gas phase, completing the reaction pathway. Fig. 8b shows the reaction pathway for the O-down NO_2 configuration, where the O-C bond length progressively increases until cleavage at 79.5 kJ/mol, followed by NO release into the gas phase after overcoming a 7.6 kJ/mol energy barrier. After NO_2 is oxidized at sites adjacent to hydroxyl groups, a portion of the NO_2 directly desorbs and undergoes subsequent adsorption and conversion reactions, while another portion remains on the active sites. During regeneration, both N-down and O-down NO_2 configurations decompose to release NO, leaving oxygen atoms bonded to carbon sites. These carbon atoms, already hydrogen-terminated, form thermally labile C-O bonds that desorb at 500 °C, thereby regenerating the active sites. Therefore, the active atoms in the vicinity of the hydroxyl functional group can be recovered during the adsorption regeneration process.

The active atoms near the carbonyl and ether groups of the oxygen-containing functional groups are discussed next. Literature reviews [34,35] indicate that ether groups within oxygen-containing functional groups decompose at approximately 600℃, while carbonyl groups decompose within a temperature range of 500–900℃. As a result, during the temperature-programmed heating of activated carbon to 500℃, neither ether nor carbonyl groups on the surface are thermally decomposed. Consequently, the number of NO_x adsorption sites near these two types of oxygen-containing functional groups remains stable throughout multiple adsorption-regeneration cycles. Calculations revealed that active atoms near carbonyl groups adsorb NO_2, forming both N-down and O-down configurations. These NO_2 species are unable to decompose into NO gas and are directly released. The energy required for desorption corresponds to the negative of their adsorption energies, with values of 32.53 kJ/mol and − 99.66 kJ/mol for the N-down and O-down adsorption configuration of NO_2, respectively. Active atoms near ether groups adsorb NO_2, forming both N-down and O-down adsorption configurations of NO_2, which are directly released without decomposing into NO gas. The desorption energies for these configurations are 173.9 kJ/mol and 182.8 kJ/mol, respectively. At a regeneration temperature of 500℃, the NO_2 adsorbed on active atoms near both carbonyl and ether groups is completely desorbed, allowing the active sites on these groups to recover during the regeneration process.

For unsaturated carbon atoms in the adsorption site, NO_2 adsorbs at

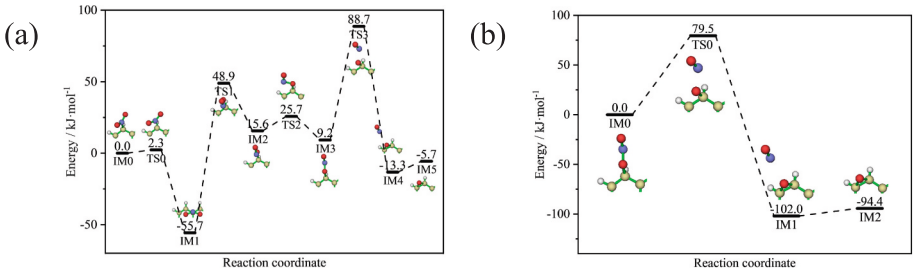

Fig. 8. Reaction pathways of (a) C-NO_2 and (b) C-ONO decomposition releasing NO on active atoms adjacent to the hydroxyl group.

the site to form N-down and O-down adsorption configurations of NO_2. Because of the strong electron-deficient nature of the sp^2 carbon of the unsaturated carbon atom, the chemical bond formed between NO_2 adsorbed at this site and the unsaturated carbon atom is stable and more difficult to break, with the required energy of 384.17–516.4 kJ/mol. By calculation, the reaction path of NO release by decomposition of N-down adsorbed and O-down adsorbed NO_2 on unsaturated carbon atoms is shown in Fig. 9. For the N-down adsorption configuration of NO_2 (Fig. 9a), an initial energy barrier of 258.8 kJ/mol must be overcome to form intermediate IM1, followed by N-O bond elongation and subsequent cleavage at 43.5 kJ/mol to produce IM2. The final NO release into the gas phase requires overcoming an 83.8 kJ/mol barrier. In contrast, the O-down adsorption configuration of NO_2 (Fig. 9b) undergoes direct N-O bond rupture at 43.5 kJ/mol, followed by NO desorption at 83.8 kJ/mol. These results demonstrate that NO release from the N-down configuration requires significantly higher energy (258.8 kJ/mol) compared to the O-down configuration (83.8 kJ/mol). Following NO release from both N-down and O-down adsorption configurations of NO_2, the residual oxygen atoms form strong C=O bonds (1.236 Å bond length, about 720 kJ/mol bond energy) with the unsaturated carbon sites. These bonds exhibit exceptional thermal stability, remaining intact at the 500℃-regeneration temperature due to their significantly higher bond energy compared to other NO_x adsorption configurations. The irreversible formation of these stable C=O structures permanently occupies the desorption sites, rendering them deactive for subsequent NO_2 chemisorption. With more adsorption regeneration cycles, the number of unsaturated carbon atoms decreases due to their occupation by the strongly bonded C=O structure. Therefore, the amount of NO_2 chemisorption that can be provided at this site will also decrease.

For saturated carbon atoms in NO_x adsorption sites, in conjunction with the literature [16], there are NO_x adsorption configurations in this class of active sites: N-down adsorption configuration of NO_2, O-down adsorption configuration of NO_2, and adsorbed NO_3^-. For N-down adsorbed NO_2 and O-down adsorbed NO_2, on the one hand, they can be directly desorbed as NO_2 with the required energy ranging from −68.9 to −60.4 kJ/mol. on the other hand, it was calculated that N-down adsorbed NO_2 and O-down adsorbed NO_2 on saturated carbon atoms can be decomposed to release NO, respectively, and the pathways are shown in Figs. 10a and b. For the N-down adsorption configuration of NO_2 (Fig. 10a), sequential energy barriers of 2.5 and 70.2 kJ/mol were overcome to form intermediate IM2, followed by N-O bond elongation and cleavage at 80.8 kJ/mol (yielding IM3), with final NO release requiring 7.5 kJ/mol. The O-down adsorption configuration of NO_2 (Fig. 10b) exhibited direct N-O bond rupture at 80.8 kJ/mol, followed by identical NO desorption (7.5 kJ/mol). For adsorbed NO_3^-, it is able to decompose to release NO_2, and the reaction path is shown in Fig. 10c. The decomposition pathway for adsorbed NO_3^- (Fig. 10c) involves N-O bond elongation followed by cleavage at 71.9 kJ/mol, with subsequent NO_2 release requiring 6.2 kJ/mol. Following decomposition, the residual oxygen forms relatively weak C-O bonds with hydrogen-saturated carbon atoms, which are susceptible to thermal cleavage at 500℃ regeneration temperatures. Then NO_x adsorption sites were recovered. Therefore, during multiple adsorption and regeneration processes, NO_x adsorbed on saturated carbon atoms are desorbed, and active sites are recovered.

Quantum chemical calculations revealed that the reduction in chemisorbed NO_x on the activated carbon surface during cyclic processes is attributed to the gradual occupation of unsaturated carbon atoms by strong C=O bonds, leading to a decrease in their availability over successive adsorption-regeneration cycles. The active atoms near the oxygen-containing functional groups (hydroxyl, carbonyl, and ether groups) are effectively restored during regeneration, and the functional groups themselves are relatively stable and do not decrease in number during the adsorption-regeneration cycle. Since saturated carbon atoms are more abundant and the active site can also be restored during regeneration, the active atoms near oxygen-containing functional groups (carbonyl, hydroxyl, and ether groups) as well as the saturated carbon atoms are not the active sites responsible for the reduction of chemisorbed NO_x due to the cyclic process of adsorption and regeneration. NO_x decomposes at unsaturated carbon sites to form stable C=O structures (bond energy of 720 kJ/mol), which cannot be thermally decomposed and restored during regeneration at 500℃, resulting in permanent deactivation of active sites. The reduction of unsaturated carbon atoms during adsorption-regeneration cycles is identified as the primary cause of decreased NO_x adsorption capacity of activated carbon. The findings provide insights into the variations in the adsorption capacity of activated carbon subjected to multiple adsorption-regeneration cycles in industrial processes. Furthermore, surface modification can be

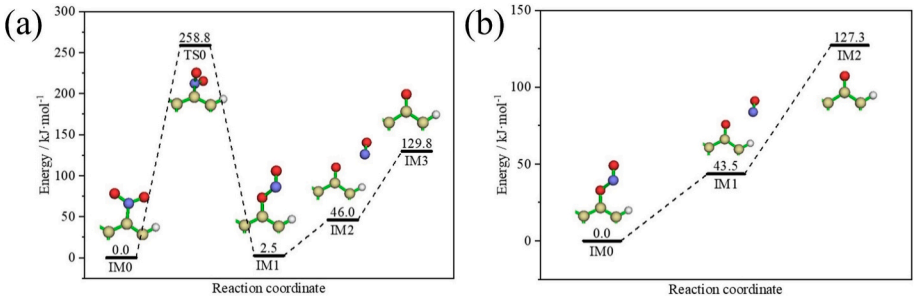

Fig. 9. Reaction pathways of (a) C-NO_2 and (b) C-ONO decomposition releasing NO on unsaturated carbon atoms.

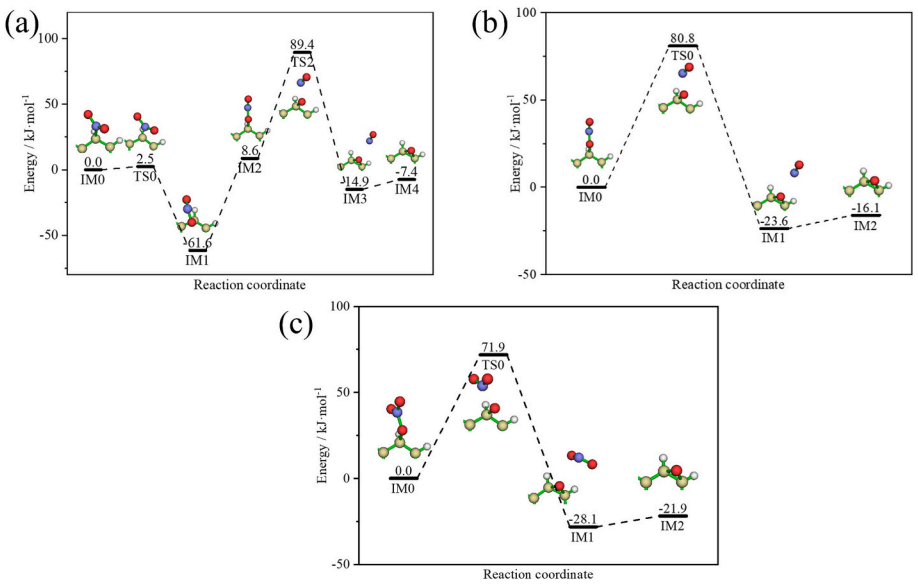

Fig. 10. Reaction pathways of (a) C-NO_2 and (b) C-ONO decomposition releasing NO, and (c) C-NO_3 decomposition releasing NO_2 on saturated carbon atoms.

employed to increase the number of NO_x active sites unaffected by cycling, thereby ensuring the stability of activated carbon's adsorption performance throughout successive adsorption-regeneration operations.

4. Conclusion

Adsorption experiments were conducted at −20℃, followed by regeneration through temperature programming to 500℃. The NO_x adsorption amount decreased by 0.262 mmol/g (11.4 %) during the first four cycles and subsequently remained nearly unchanged, reaching a stable state. During the cycling process, the reduction in chemisorption amount accounted for 84.7 % of the total decrease in adsorption amount, with the decline in NO_x adsorption primarily attributed to changes in chemisorption. The physical adsorption of NO_x showed only a slight decrease during the first adsorption-regeneration cycle and remained nearly unchanged in subsequent cycles.

Further analysis of the temperature-programmed desorption (TPD) curves for activated carbon samples subjected to varying numbers of adsorption-regeneration cycles revealed a gradual decrease and stabilization of the NO desorption peak, whereas the NO_2 desorption peak remained largely unchanged. These observations, in conjunction with prior research, indicate the presence of a specific type of NO_x adsorption site on the activated carbon surface that diminishes progressively with successive adsorption-regeneration cycles, leading to a continuous reduction in NO_x adsorption amount. Characterization of the physical characteristics of activated carbon subjected to varying numbers of adsorption-regeneration cycles revealed a reduction in average pore size following the first cycle, leading to slower diffusion rates and a slight decrease in the physical adsorption of NO_x. In subsequent cycles, the physical properties of the activated carbon remained largely unchanged, resulting in minimal variation in the physical adsorption of NO_x. XPS characterization of activated carbon subjected to varying adsorption-regeneration cycles revealed the presence of surface functional groups, including carbonyl, hydroxyl, ether groups, and carbon edge defects. The progression of adsorption-regeneration cycles led to a significant reduction in carbon edge defects adsorption sites, while C-O–H (hydroxyl) groups remained relatively unchanged. Combined with the analysis of temperature-programmed desorption experiments, it is concluded that the cycles exert negligible influence on both the hydroxyl functional groups and the NO oxidation reactions on the activated carbon surface.

Activated carbon exhibits negligible direct NO adsorption capacity, relying instead on a two-step process involving NO oxidation followed by NO_2 conversion. XPS characterization, combined with the results of temperature-programmed desorption experiments, indicates that adsorption-regeneration cycles have minimal impact on the NO oxidation stages on the activated carbon surface. The observed decrease in total adsorption amount (84.7 % attributable to chemisorption decline) was investigated through quantum chemical calculations of three primary NO_2 adsorption sites: oxygen-functional groups (hydroxyl, carbonyl, ether), unsaturated carbon atoms, and saturated carbon atoms. The active atoms adjacent to the oxygen-containing functional groups (hydroxyl, carbonyl, and ether groups) can be effectively restored during the regeneration process, and the functional groups themselves are relatively stable, and their number will not decrease in the adsorption and regeneration cycle. The saturated carbon atoms are more abundant and the active sites can also be recovered during regeneration, so the active atoms near the oxygen-containing functional groups (carbonyl, hydroxyl, and ether groups) and the saturated carbon atoms are not the sites that are responsible for the decrease of chemisorbed NO_x on the surface of activated carbon during the adsorption-regeneration cycles. NO_x forms a strongly bonded C=O structure (bond energy 720 kJ/mol) after decomposition of the unsaturated carbon sites, which cannot be recovered by pyrolysis during regeneration at 500℃, resulting in permanent deactivation of the active sites. The decrease in adsorption on the activated carbon surface during the adsorption-regeneration cycle is caused by the reduction of unsaturated carbon atoms.

The research findings aid in understanding the variation in adsorption performance of activated carbon during multiple adsorption-regeneration cycles in industrial processes. Furthermore, surface modification can be utilized to enhance the number of NO_x active sites unaffected by cycling, thereby ensuring the stability of activated carbon's adsorption performance throughout adsorption-regeneration operations.

CRediT authorship contribution statement

Zhongwei Li: Writing – review & editing, Writing – original draft, Visualization, Validation, Software, Methodology, Investigation, Formal analysis, Data curation, Conceptualization. **Xingyu Yang:** Writing – review & editing, Validation, Software, Methodology, Conceptualization. **Qiang Song:** Writing – review & editing, Supervision, Project administration, Conceptualization.

Declaration of competing interest

The authors declare that they have no known competing financial interests or personal relationships that could have appeared to influence the work reported in this paper.

Acknowledgements

This work was supported by the National Key Research and Development Program of China (2022YFB4100201), National Natural Science Foundation of China (51976103) and the Fundamental Research Funds for the Central Universities of China (2022ZFJH04).

Data availability

Data will be made available on request.

References

[1] I. Potykova, L. Obalova, L. Kubonova, K. Obroucka, The balancing of NO concentration fluctuations by adsorption/desorption process on activated carbon, Sep. Purif. Technol. 78 (2011) 245–248, https://doi.org/10.1016/j.seppur.2011.01.035.
[2] S. Wei-yi, W. Qing-yuan, D. Sang-lan, S. Shi-jun, J. Wen-ju, Z. Er-gang, Reaction mechanism of NO_x removal from flue gas with pyrolusite slurry, Sep. Purif. Technol. 118 (2013) 576–582, https://doi.org/10.1016/j.seppur.2013.08.005.
[3] L. Yang, M. Shen, F. Gao, W. Li, G. Shen, X. Li, Mn loading effects on MnO_x/$CeZrO_x$ low temperature passive NO_x adsorbers, Sep. Purif. Technol. 361 (2025) 131483, https://doi.org/10.1016/j.seppur.2025.131483.
[4] D. Damma, P.R. Ettireddy, B.M. Reddy, P.G. Smirniotis, A Review of low temperature NH_3-SCR for removal of NO_x, Catalysts 9 (2019) 349, https://doi.org/10.3390/catal9040349.
[5] G. Busca, L. Lietti, G. Ramis, F. Berti, Chemical and mechanistic aspects of the selective catalytic reduction of NO_x by ammonia over oxide catalysts: a review, Appl. Catal. B-Environ. 18 (1998) 1–36, https://doi.org/10.1016/S0926-3373(98)00040-X.
[6] P. Forzatti, Present status and perspectives in de-NO_x SCR catalysis, Appl. Catal. A-Gen., 222 (2001) 221-236. ttps://doi.org/10.1016/S0926-860X(01)00832-8.
[7] G. Madia, M. Elsener, M. Koebel, F. Raimondi, A. Wokaun, Thermal stability of vanadia-tungsta-titania catalysts in the SCR process, Appl. Catal. B-Environ. 39 (2002) 181–190, https://doi.org/10.1016/S0926-3373(02)00099-1.
[8] V.I. Pârvulescu, P. Grange, B. Delmon, Catalytic removal of NO, Catal. Today 46 (1998) 233–316, https://doi.org/10.1016/S0920-5861(98)00399-X.
[9] Y. Zheng, A.D. Jensen, J.E. Johnsson, Deactivation of V_2O_5-WO_3-TiO_2 SCR catalyst at a biomass-fired combined heat and power plant, Appl. Catal. B-Environ. 60 (2005) 253–264, https://doi.org/10.1016/j.apcatb.2005.03.010.
[10] Y.W. Lee, D.K. Choi, J.W. Park, Characteristics of NO_x adsorption and surface chemistry on impregnated activated carbon, Sep. Sci. Technol. 37 (2002) 937–956, https://doi.org/10.1081/SS-120002224.
[11] S. Sumathi, S. Bhatia, K.T. Lee, A.R. Mohamed, Performance of an activated carbon made from waste palm shell in simultaneous adsorption of SO_x and NO_x of flue gas at low temperature, Science in China Series E-Technological, Sciences 52 (2009) 198–203, https://doi.org/10.1007/s11431-009-0031-6.
[12] N. Ahmad, N. Ibrahim, U.F.M. Ali, S.Y. Yusuf, F.M. Ridwan, Carbon-supported CuO Catalyst Prepared from Oil Palm Empty Fruit Bunch (EFB) for Low-Temperature No Removal, in: 4th International Conference on Process Engineering and Advanced Materials (ICPEAM), Kuala Lumpur, Malaysia, 2016, pp. 823-829.
[13] F.-T. You, G.-W. Yu, Y. Wang, Z.-J. Xing, X.-J. Liu, J. Li, Study of nitric oxide catalytic oxidation on manganese oxides-loaded activated carbon at low temperature, Appl. Surf. Sci. 413 (2017) 387–397, https://doi.org/10.1016/j.apsusc.2017.04.044.
[14] Y. Zhuang, X. Liu, H. Hua, Y. Su, Z. Hou, Z. Zhou, Y. Ji, X. Jiao, X. Yu, Y. Zhang, Progress in hydrophobic or superhydrophobic modification of activated carbon, Surf. Technol. 53 (2024) 1–17, https://doi.org/10.16490/j.cnki.issn.1001-3660.2024.05.001.
[15] S. Wang, S. Xu, S. Gao, P. Xiao, M. Jiang, H. Zhao, B. Huang, L. Liu, H. Niu, J. Wang, D. Guo, Simultaneous removal of SO_2 and NO_x from flue gas by low-temperature adsorption over activated carbon, Sci. Rep. 11 (2021) 11003, https://doi.org/10.1038/s41598-021-90532-9.
[16] Z. Li, G. Song, X. Yang, Q. Song, Mechanism of O_2-promoted NO adsorption on activated carbon: an experimental and computational study, Chem. Eng. J. 481 (2024) 148391, https://doi.org/10.1016/j.cej.2023.148391.
[17] Z. Li, X. Yang, Y. Wang, H. Yang, Q. Song, Characteristics and mechanism of low-temperature NO adsorption by activated carbon, Chem. Eng. J. 495 (2024) 153639, https://doi.org/10.1016/j.cej.2024.153639.
[18] E. Raymundo-Piñero, D. Cazorla-Amorós, A. Linares-Solano, Temperature programmed desorption study on the mechanism of SO_2 oxidation by activated carbon and activated carbon fibres, Carbon 39 (2001) 231–242, https://doi.org/10.1016/S0008-6223(00)00119-6.
[19] Y. Guo, Y. Li, T. Zhu, M. Ye, Investigation of SO_2 and NO adsorption species on activated carbon and the mechanism of NO promotion effect on SO_2, Fuel, 143 (2015) 536-542. ttps://doi.org/10.1016/j.fuel.2014.11.084.
[20] F.-T. You, G.-W. Yu, Z.-J. Xing, J. Li, S.-Y. Xie, C.-X. Li, G. Wang, H.-Y. Ren, Y. Wang, Enhancement of NO catalytic oxidation on activated carbon at room temperature by nitric acid hydrothermal treatment, Appl. Surf. Sci. 471 (2019) 633–644, https://doi.org/10.1016/j.apsusc.2018.12.066.
[21] R. Zhang, F. Gao, X. Tang, H. Yi, Y. Zhou, Temperature responses of two synergistic pathways for low-temperature catalytic oxidation of high-concentration NO over ACFs: nano-confinement and nitrogen-containing groups, Fuel 325 (2022) 124878, https://doi.org/10.1016/j.fuel.2022.124878.
[22] Z. Zhang, J.D. Atkinson, B. Jiang, M.J. Rood, Z. Yan, Nitric oxide oxidation catalyzed by microporous activated carbon fiber cloth: an updated reaction mechanism, Appl. Catal. B-Environ. 148–149 (2014) 573–581, https://doi.org/10.1016/j.apcatb.2013.10.050.
[23] J.D. Atkinson, Z. Zhang, Z. Yan, M.J. Rood, Evolution and impact of acidic oxygen functional groups on activated carbon fiber cloth during NO oxidation, Carbon 54 (2013) 444–453, https://doi.org/10.1016/j.carbon.2012.11.060.
[24] X. Zhu, L. Zhang, T. Wang, J. Li, X. Zhou, C. Ma, Y. Dong, An updated study on NO catalytic oxidation over activated carbon: the effect of pore structure and a dual-site mechanism, Fuel 311 (2022) 122627, https://doi.org/10.1016/j.fuel.2021.122627.
[25] A.P. Terzyk, The influence of activated carbon surface chemical composition on the adsorption of acetaminophen (paracetamol) in vitro: Part II. TG, FTIR, and XPS analysis of carbons and the temperature dependence of adsorption kinetics at the neutral pH, Colloids Surf. A 177 (2001) 23–45, https://doi.org/10.1016/S0927-7757(00)00594-X.
[26] J. Wang, M. Yang, D. Deng, S. Qiu, The adsorption of NO, NH_3, N_2 on carbon surface: a density functional theory study, J. Mol. Model. 23 (2017) 262, https://doi.org/10.1007/s00894-017-3429-2.
[27] X. Pi, F. Sun, J. Gao, Z. Qu, A. Wang, Z. Qie, L. Wang, H. Liu, A new insight into the SO_2 adsorption behavior of oxidized carbon materials using model adsorbents and DFT calculations, PCCP 21 (2019) 9181–9188, https://doi.org/10.1039/C8CP07782G.
[28] X. Zhu, L. Zhang, M. Zhang, C. Ma, Effect of N-doping on NO_2 adsorption and reduction over activated carbon: an experimental and computational study, Fuel 258 (2019) 116109, https://doi.org/10.1016/j.fuel.2019.116109.
[29] Z. Qu, F. Sun, J. Gao, X. Pi, Z. Qie, G. Zhao, A new insight into SO_2 low-temperature catalytic oxidation in porous carbon materials: non-dissociated O_2 molecule as oxidant, Catal, Sci. Technol. 9 (2019) 4327–4338, https://doi.org/10.1039/C9CY00960D.
[30] Z. Li, W. Zhang, Z. Chen, Q. Zhang, X. Yang, S. Mao, W. Jian, Reaction mechanism for NO oxidation on the soot surface using a quantum chemistry, Fuel 313 (2022) 123032, https://doi.org/10.1016/j.fuel.2021.123032.
[31] Z. Qu, F. Sun, X. Pi, X. Li, D. Wu, J. Gao, G. Zhao, One-step synergistic optimization of hierarchical pore topology and nitrogen dopants in activated coke for efficient catalytic oxidation of nitric oxide, J. Cleaner Prod. 335 (2022) 130360, https://doi.org/10.1016/j.jclepro.2022.130360.
[32] M. Frisch, G. Trucks, H.B. Schlegel, G. Scuseria, M. Robb, J. Cheeseman, G. Scalmani, V. Barone, G. Petersson, H. Nakatsuji, Gaussian 16, in, Gaussian, Inc., Wallingford, CT, 2016.
[33] T. Lu, F. Chen, Multiwfn: a multifunctional wavefunction analyzer, J. Comput. Chem. 33 (2012) 580–592, https://doi.org/10.4209/aaqr.2018.07.0269.
[34] S. Liu, X. Yu, G. Lin, R. Qu, C. Zheng, X. Gao, Insights into the effect of adsorption–desorption cycles on SO_2 removal over an activated carbon, aerosol air, Qual. Res. 19 (2019) 411–421.
[35] J. Li, L. Zhang, X. Zhao, M. Zhang, T. Feng, B. Zhou, T. Wang, Z. Song, C. Ma, Insights into the effect of regeneration temperature on physicochemical properties and SO_2 removal over powdered activated coke, Fuel 288 (2021) 119715, https://doi.org/10.1016/j.fuel.2020.119715.
[36] Z. Li, X. Yang, Q. Song, Inhibition of SO_2 for low-temperature NO adsorption on activated carbon, Energy Fuels 38 (2024) 20994–21003, https://doi.org/10.1021/acs.energyfuels.4c03991.